J. Min. Metall. Sect. B-Metall. 48 (3) B (2012) 403 - 411

Journal of Mining and Metallurgy, Section B: Metallurgy

EVOLUTION OF SECONDARY PHASES IN 0.17C-16Cr-11Mn-0.43N AUSTENITIC STAINLESS STEEL AT 800 AND 850°C - THERMODYNAMIC MODELING OF PHASE EQUILIBRIA AND EXPERIMENTAL KINETIC STUDIES

R. Čička[a], J. Bakajová[b], M. Štefániková[a], M. Dománková[a], J. Janovec[a]

[a] Slovak University of Technology in Bratislava, Faculty of Materials Science and Technology in Trnava, Slovak Republic
[b] Welding Research Institute – Industrial Institute of the Slovak Republic, Bratislava, Slovak Republic

(Received 02 July 2012; accepted 27 October 2012)

Abstract

The precipitation of secondary phases was investigated in the 0.17C-16Cr-11Mn-0.43N austenitic stainless steel during annealing at 800 and 850°C for times between 5 min and 100 h. Light microscopy, transmission electron microscopy, energy dispersive X-ray spectroscopy, scanning electron microscopy, and differential thermal analysis were used in experiments. Thermodynamic calculations were done by the Thermo-Calc database software package. Cr_2N and $M_{23}C_6$ were considered to be stable phases at the annealing temperatures. Cells consisting of alternating Cr_2N and austenite lamellae were observed in the steel microstructure after sufficiently long annealing. The metastable chi phase was also found in all the annealed samples. After 100 h of annealing the equilibrium sigma started to precipitate. The thermodynamically predicted M_6C was not confirmed experimentally in any of the annealed samples. DTA analysis showed the initial precipitation stage was followed by the phase dissolution. For the investigated steel the computational thermodynamics can be used only for qualitative interpretation of the experimental results as the measured endothermal peaks were found to be shifted of about 50 ÷ 70 °C related to the computed results.

Keywords: *Austenitic stainless steel; Secondary phases; Thermodynamic modeling; Transmission electron microscopy*

1. Introduction

Newly designed austenitic stainless steels (ASSs) for low temperature applications with improved mechanical properties and better corrosion resistance were developed recently by modifications in the steel bulk composition [1-4]. However, compositional changes in the bulk were also found to influence precipitation sequences of secondary phases [5-8]. A special group between ASSs are high-nitrogen chromium-manganese steels, marked also CrMnN [9-12]. Besides improved mechanical properties and corrosion resistance at low-temperatures they exhibit also an enhanced biocompatibility due to the replacement of nickel with nitrogen and manganese [9-12].

There are differences between Cr-Ni and CrMnN ASSs in the precipitation behaviour at higher temperatures. While the former steels show only negligible changes in morphology, structure, and metal composition of secondary phase particles on annealing at temperatures between 700 and 1000°C, the latter steels overcome an intensive precipitation in this temperature range [13,14]. $M_{23}C_6$ is the typical secondary phase in majority of the Cr-containing ASSs. Intergranular particles of this phase initiate mostly the susceptibility to intergranular embrittlement and corrosion [15]. In the steels with limited carbon content sigma and chi phases are also present in the form of massive particles mostly along the grain boundaries. Chi was also observed inside the grains in ASSs containing transition metals, e.g. molybdenum [7,13]. Chi as metastable phase transforms mostly into sigma during annealing [16]. $M_{23}C_6$ was also reported to precede the sigma formation at the grain boundaries [17]. Cr_2N precipitates in CrMnN ASSs usually after long-term annealing [18]. Mostly it is a part of cells (called also "nitrogen pearlite") containing alternating lamellae of Cr_2N and austenite [2,19-21]. Particles of Cr_2N start to precipitate at the grain boundaries and subsequently grow towards the grain interior forming nitrogen pearlite [22,23]. The formation of nitrogen-depleted zones near Cr_2N particles was found to support the sigma precipitation in the vicinity of nitrogen pearlite [8].

* *Corresponding author: roman.cicka@stuba.sk*

DOI:10.2298/JMMB120702051C

Dedicated to the memory of Professor Zbigniew Moser

The main aim of this work is to quantify the influence of annealing conditions on the precipitation behaviour of the 0.2C-18Cr-10Mn-0.5N steel. Both experimental techniques and thermodynamic calculations were used for the structural and compositional characterization of precipitating secondary phases.

2. Experimental

The investigated 0.17C-16Cr-11Mn-0.43N steel (for chemical composition see Table 1) was solution heat-treated at 1100°C for 0.5 h, subsequently cooled to room temperature, and finally annealed at either 800 or 850°C for 5 min, 10 min, 30 min, 60 min, 4 h, 10 h, 30 h and 100 h.

The specimens for light microscopy (LM) were polished, electrolytically etched using 10% oxalic acid at the current density of 1 $A.cm^{-2}$, and documented using a NEOPHOT 32 microscope equipped with a CCD camera. The linear intercept segment method was used to determine the average grain size.

For the scanning electron microscopy (SEM) observations a JEOL JSM-7600F microscope was used operating at acceleration voltage 20 kV. A JEOL 200CX microscope operating at 200 kV was used for the transmission electron microscopy (TEM) observations. Secondary phase particles extracted into carbon replicas were identified by the selected area electron diffraction (SAED), metal compositions of them were determined by energy dispersive X-ray spectroscopy (EDX) using software for thin samples. No corrections for absorption or fluorescence were made in the investigation.

The differential thermal analysis (DTA) was done with a Netzsch STA 409 CD under protective argon atmosphere (40 ml/min). Thermal effects corresponding to phase transitions were recorded at linear heating rate of 10 K/min.

Thermodynamic calculations were performed by the Thermo-Calc software working with the TCFE6 database [24]. For the thermodynamic description of phases the sublattice model was used. This model makes possible to consider the mixing of defined components at each sublattice and enables also to calculate the particular contributions to the phase Gibbs free energy [25]. The calculations of phase equilibria (stable or metastable) are based on the Gibbs free energy minimization. Moreover, important thermodynamic quantities (molar fractions of phases, compositions of phases, Gibbs free energy, Helmholtz free energy, enthalpy, entropy, heat capacity, expansion coefficient, …) can be easily calculated for the system and/or individual phases, usually in dependence on temperature [26].

In the present work, phase equilibria and both molar factions and metal compositions of equilibrium phases were calculated for the system corresponding to the investigated 0.17C-16Cr-11Mn-0.43N steel in the temperature range of 300-1200°C. In the calculations, Fe, Cr, Mo, Mn, Si, C, N as elements and austenite (FCC_A1), Cr_2N (HCP_A3), $M_{23}C_6$, M_7C_3, M_6C, chi (CHI), and sigma (SIGMA) as representative phases occurring in ASSs were considered.

3. Results

The microstructure of the investigated steel after solution heat treatment was found to consist of polyhedral austenitic grains with the average grain size of 40 μm (Fig. 1a). The annealing led to the secondary phase precipitation and the cell formation (Figs. 1b and 2). Only negligible changes were observed between the microstructures annealed for the same time at different temperatures (800 and 850°C). Amount of precipitates was found to increase with increasing the annealing time.

In the austenitic matrix, mostly large secondary phase particles (linear dimension higher than 1 μm) of various types and morphologies were identified. The occurrence of $M_{23}C_6$ (Fig. 3), chi (Fig. 4), Cr_2N (Fig. 5), and sigma (Fig. 6) in annealed samples is summarized in Table 2. The calculated phase equilibria for 800 and 850°C are also given in Table 2 (see the bottom row) to make possible their comparison with the experimental results. In Figs. 3-6 couples of images are illustrated showing morphology of the analysed particle and its SAED pattern.

Using the EDX/TEM technique, Cr, Mo, Fe and traces of Mn and Ni were found in analysed particles of $M_{23}C_6$, chi and Cr_2N. These phases were found to be the dominant secondary phases in the investigated steel (Table 2) identified almost in all the experimental conditions. The experimentally determined contents of Cr, Fe, and Mo in $M_{23}C_6$, chi, Cr_2N, and sigma and the calculated equilibrium values are compared in Figs. 7a and 7b for annealing temperatures 800 and 850°C, respectively. The experimentally determined metal contents for particular phases are marked with empty symbols of various shapes (for the detail description see figure

Table 1. *Chemical composition of investigated 0.17C-16Cr-11Mn-0.43N steel. Mass contents of elements are given in %*

C	Si	Mn	Cr	Mo	W	Ni	Al	P	S	N	Fe
0.17	0.53	10.62	16.13	3.79	0.12	0.01	0.008	0.003	0.004	0.43	bal.

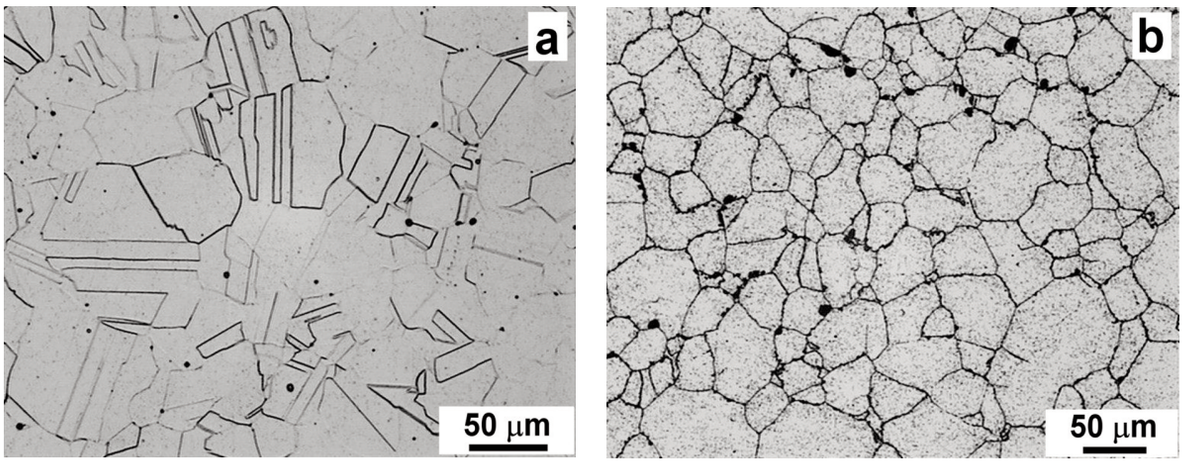

Figure 1. *Microstructures of the 0.17C-16Cr-11Mn-0.43N steel after solution heat treatment (a) and annealing of the solution heat-treated sample at 800°C for 4 h (b), LM*

Table 2. *Secondary phases identified experimentally in particular conditions of the 0.17C-16Cr-11Mn-0.43N steel. In the bottom row the calculated phase equilibria are given*

Annealing time	Annealing temperature	
	800°C	850°C
5 min	$M_{23}C_6$, chi	$M_{23}C_6$, chi, Cr_2N
10 min	$M_{23}C_6$, chi , Cr_2N	$M_{23}C_6$, chi, Cr_2N
30 min	$M_{23}C_6$, chi, Cr_2N	$M_{23}C_6$, chi, Cr_2N
1 h	$M_{23}C_6$, chi, Cr_2N	$M_{23}C_6$, chi, Cr_2N
4 h	$M_{23}C_6$, chi, Cr_2N	$M_{23}C_6$, chi, Cr_2N
10 h	$M_{23}C_6$, chi, Cr_2N	$M_{23}C_6$, chi, Cr_2N
30 h	$M_{23}C_6$, chi, Cr_2N	$M_{23}C_6$, chi, Cr_2N
100 h	$M_{23}C_6$, chi, Cr_2N, sigma	$M_{23}C_6$, chi, Cr_2N, sigma
Calculated phase equilibria	$M_{23}C_6$, Cr_2N, sigma, M_6C	$M_{23}C_6$, Cr_2N, sigma, M_6C

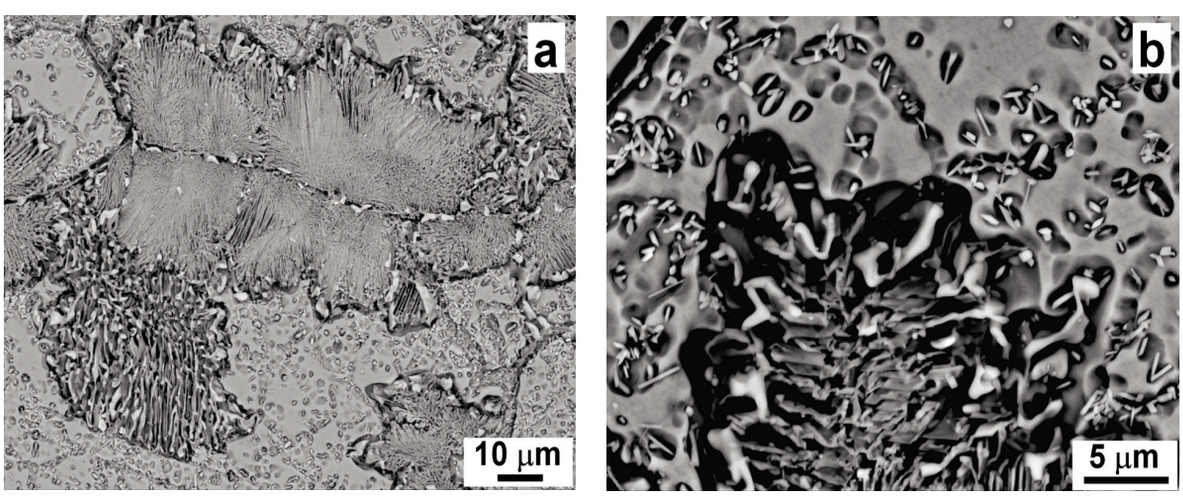

Figure 2. *Microstructure of the 0.17C-16Cr-11Mn-0.43N steel after annealing at 800°C for 100 h (a), detail view on cell/matrix interface (b), SEM*

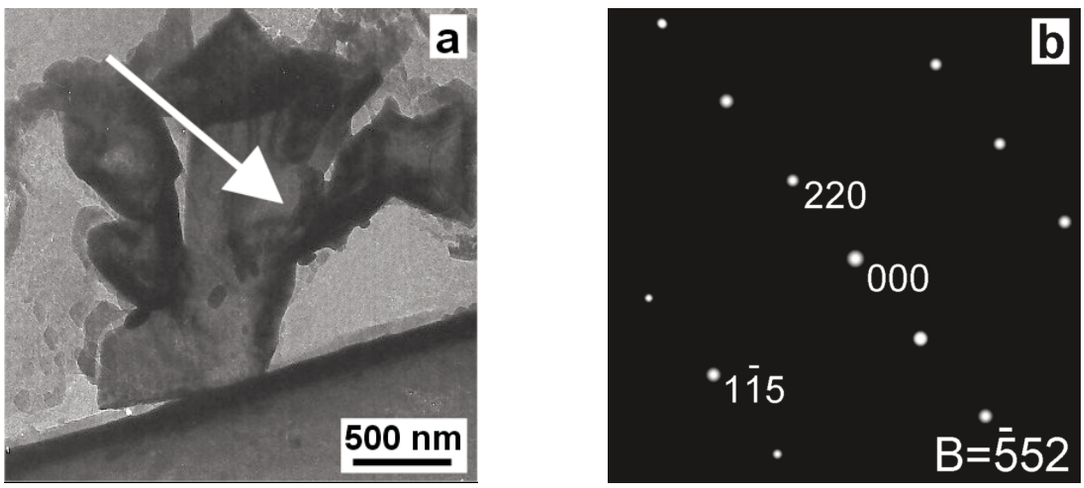

Figure 3. *Characteristic morphology of $M_{23}C_6$ particles (a), SAED pattern of the particle marked with arrow. Illustrated for the 0.17C-16Cr-11Mn-0.43N steel annealed at 850°C for 5 h (b), TEM*

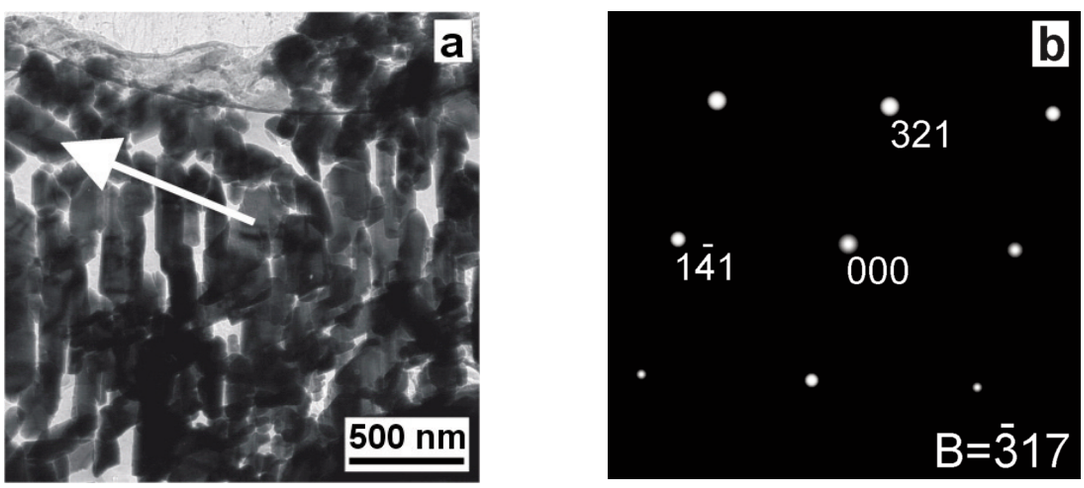

Figure 4. *Particles of chi phase near the cell/matrix interface (a), SAED pattern of the particle marked with arrow. Illustrated for the 0.17C-16Cr-11Mn-0.43N steel annealed at 800°C for 4 h (b), TEM*

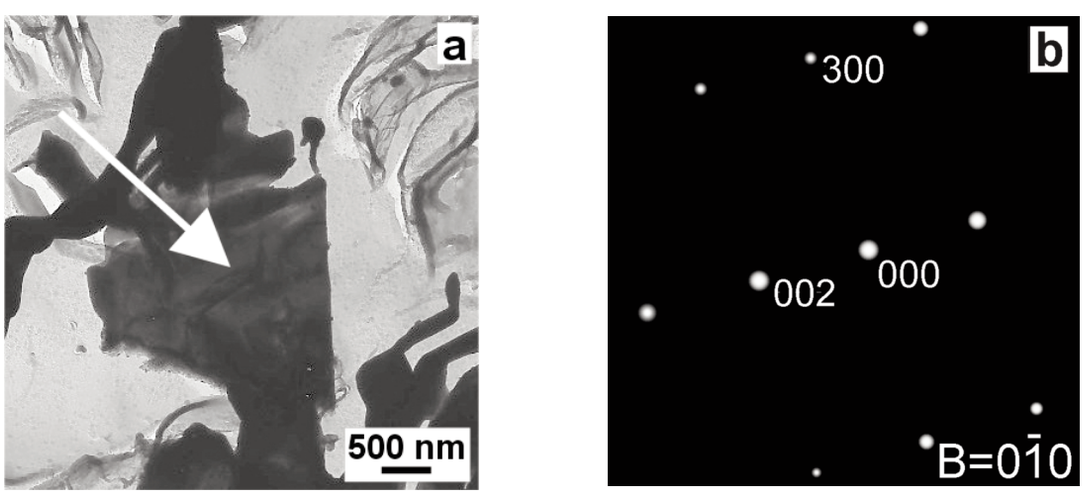

Figure 5. *Characteristic morphology of Cr_2N particles (a), SAED pattern of the particle marked with arrow. Illustrated for the 0.17C-16Cr-11Mn-0.43N steel annealed at 850°C for 30 min (b), TEM*

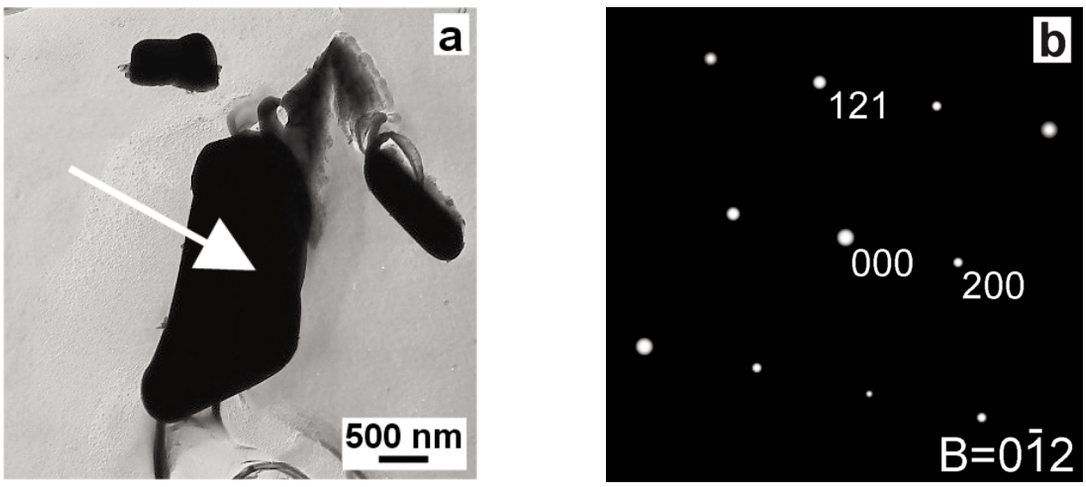

Figure 6. *Characteristic morphology of sigma particles (a), SAED pattern of the particle marked with arrow. Illustrated for the 0.17C-16Cr-11Mn-0.43N steel annealed at 850°C for 100 h (b), TEM*

captions), the calculated equilibrium values are marked with solid symbols of the identical shape. The only exception concerns the non-equilibrium chi phase, the calculated composition of which is marked by another type of symbol as used for experimentally found compositions of this phase. The reason resides in the fact that sigma was omitted in the calculation to determine the metal composition of chi. During annealing at 800 °C, the Cr content in Cr_2N increased from 66.1 to 82.4 wt.%, the Mo content decreased from 22.1 to 10.2 wt.% and the Fe content decreased from 4.7 to 2.8 wt.%. Chi was found to contain about 33 wt.% Cr, 28 wt.% Mo, and 30 wt.% Fe. Sigma at 800 °C (after 100 h of annealing) contained about 19.8 wt.% Cr, 12.8 wt.% Mo, 55 wt.% Fe. The Cr content in $M_{23}C_6$ was found to increase from 43.8 to 58.5 wt.%, the Mo content to increase from 10.8 to 16.2 wt.%, and the Fe content to decrease from 26.6 to 18.1 wt.%. The longer the annealing time, the better the agreement between experimental and calculated values of the stable phase metal composition. There were not observed any significant changes in metal compositions of secondary phase particles extracted from the samples annealed for the same time at 800 and 850 °C.

The calculated phase equilibria given in Table 2 were derived from the isopleths illustrated in Figs. 8 and 9. Austenite, Cr_2N, M_6C, $M_{23}C_6$ and sigma were predicted to be equilibrium phases in the system corresponding to the investigated 0.17C-16Cr-11Mn-0.43N steel for bulk carbon (nitrogen) contents up to 0.5 wt.% (1 wt.%).

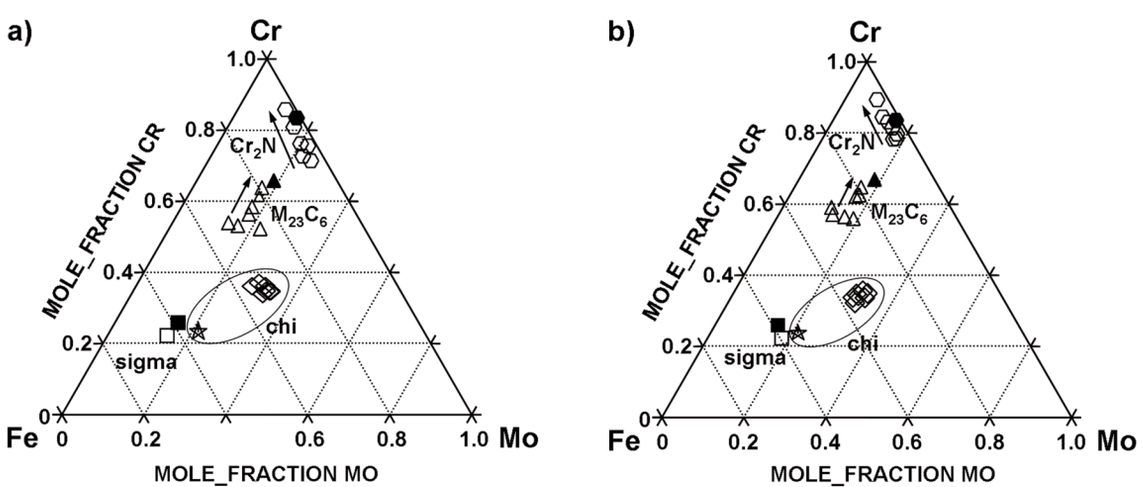

Figure 7. *Contents of Fe, Cr, and Mo in $M_{23}C_6$ (positions of the phase are marked with triangles), chi (rhombi), Cr_2N (hexagons), and sigma (squares). Empty symbols of all shapes correspond to experimental values, solid symbols correspond to calculated equilibrium values, and the five-fold star represents the calculated value for metastable chi phase. Arrows close to experimental values show the increase in annealing time for particular phases. Illustrated for 800°C (a) and 850 °C (b) (see also Table 2)*

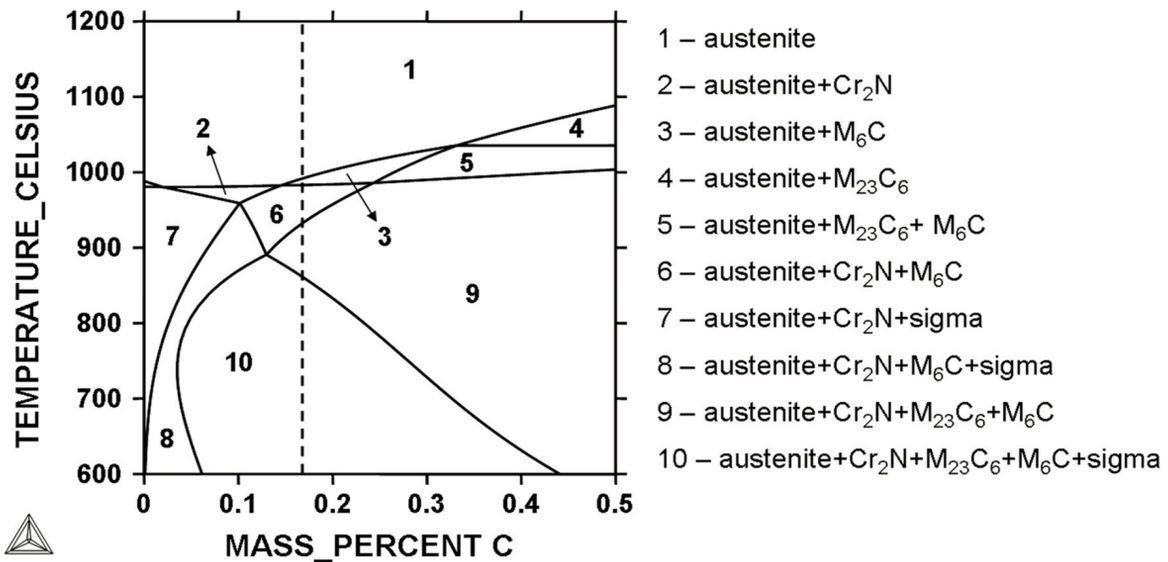

Figure 8. *Isopleth Fe-C calculated for system corresponding to the investigated 0.17C-16Cr-11Mn-0.43N steel. Dashed vertical line shows position of the investigated steel. Numbers inside the isopleth represent particular phase equilibria*

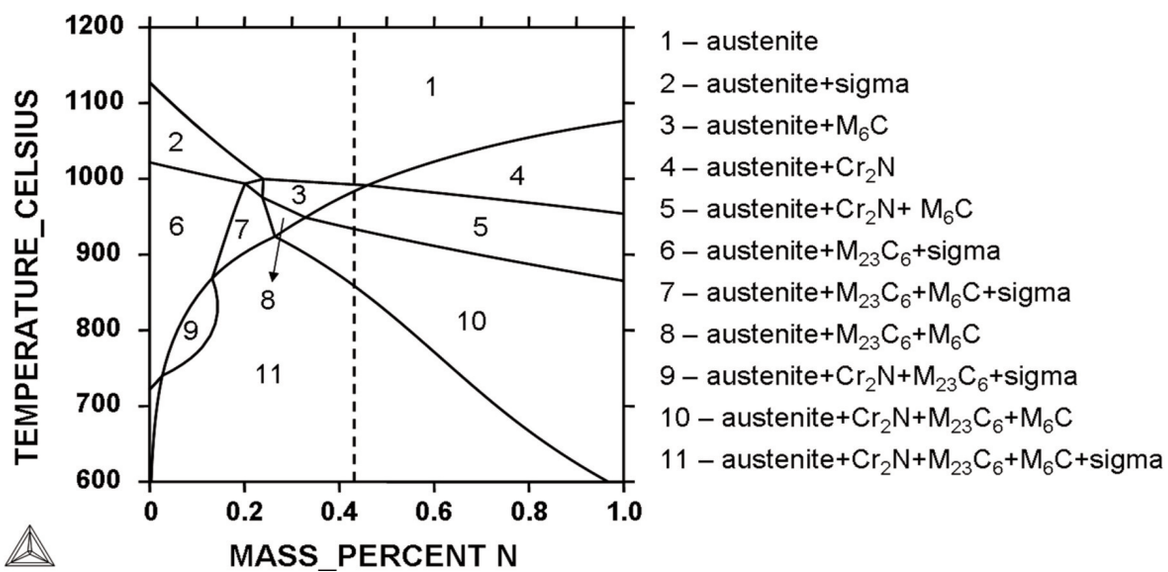

Figure 9. *Isopleth Fe-N calculated for system corresponding to the investigated 0.17C-16Cr-11Mn-0.43N steel. Dashed vertical line shows position of the investigated steel. Numbers inside the isopleth represent particular phase equilibria.*

DTA curves for the investigated steel are shown in Fig. 10. The upper curve corresponds to the originally solution heat-treated sample. The lower curve was recorded for the sample annealed at 800°C for 100 h. A slow exothermic behaviour (precipitation of secondary phases) shows upper (lower) curve up to 650°C (653°C), followed by exothermic peak at 752°C (722°C). The endothermic process (dissolution of secondary phases) was observed to start at this temperature. The first endothermic peak is shown at 890°C (888°C) and the second endothermic peak is located at 1030°C (1025°C).

4. Discussion

According to thermodynamic predictions austenite, $M_{23}C_6$, Cr_2N, M_6C and sigma are equilibrium phases at 800 and 850°C in the investigated steel. $M_{23}C_6$, Cr_2N, chi, and sigma were identified in the steel by experiment after annealing for 100 h at both the temperatures (Table 2). This shows chi is the non-equilibrium phase under given

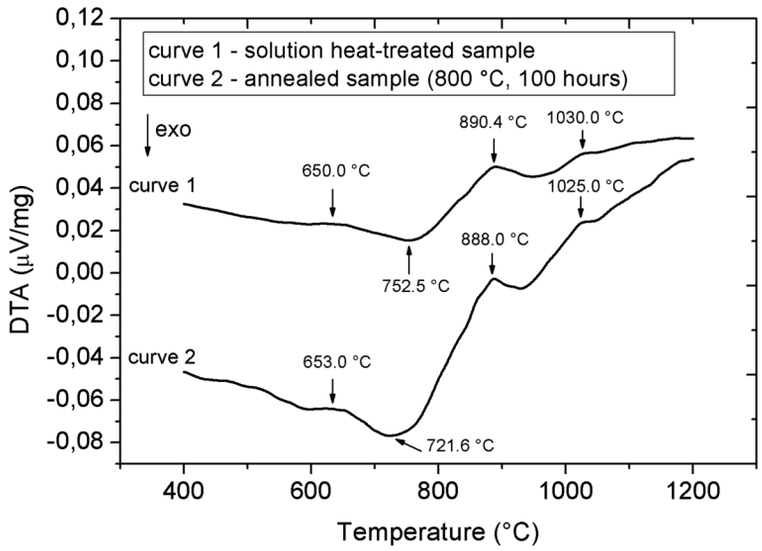

Figure 10. *DTA record of the 0.17C-16Cr-11Mn-0.43N steel. The upper curve corresponds to the originally solution heat-treated sample, the lower curve corresponds to the sample annealed at 800°C for 100 h. The samples were heated with the rate of 10 K/min*

conditions and it is expected therofore to lose its microstructural stability on prolonged annealing after sigma is formed. The above result resembles the precipitation sequence found in duplex steels, when chi is consumed at the sigma forming reaction at 750 – 950 °C [16]. M_6C was predicted as equilibrium phase in the investigated steel, but it was not found experimentally. This result is in agreement with that of Janovec et al. [27] that in certain steels M_6C can be formed after very long annealing only, nearly 1000 h at temperatures about 800 °C.

Phases $M_{23}C_6$, chi and Cr_2N are formed at the first stage of annealing at 800°C (850°C). The composition of $M_{23}C_6$ and Cr_2N is continuosly changing toward the equilibrium composition predicted by thermodynamic calculations. However, the experimentally determined composition of the metastable chi phase differs significantly from the calculated composition, and it does not change during annealing. After 100 h of annealing sigma phase starts to form. The composition of this phase is very close to predicted equilibrium composition and it is also close to predicted composition of metastable chi phase.

In microstructures of samples annealed for 100 h chi is present in the form of fine particles inside the austenitic grains, Cr_2N forms cells growing from the grain boundaries, sigma particles occur at the periphery of Cr_2N cells, and $M_{23}C_6$ was found both at the periphery of Cr_2N cells and at the grain boundaries. This type of microstructure is typical for high-nitrogen ASSs [8,13,15].

DTA measurements performed on both solution heat-treated and annealed samples show very similar behaviour of these samples. To interpret these measurements, the thermodynamic calculations of molar fractions of the phases were performed and plotted in dependence on temperature. In Fig. 11a the result of equilibrium calculation is shown being complementary to the isopleths illustrated in Figs. 8 and 9. In Fig. 11b the result of calculation is documented, in which two of the equilibrium phases not found experimentally (sigma, M_6C) were omitted. This resulted in the appearance of the metastable chi phase in the plot. At initial decreasing part of the DTA curve (Fig. 10) the precipitation of secondary phases occurs. The small diffuse exothermal peak at 650°C (653°C) superimposed at this part of the curve may be related to some changes (and partial dissolution) of the metastable chi phase. At 753°C (722°C) the dissolution of chi continues and a slow dissolution of other secondary phases ($M_{23}C_6$, Cr_2N) starts. It is in agreement with the calculated results shown in Fig.11b, where the curves of $M_{23}C_6$ and Cr_2N start to decrease at similar temperatures. The next two endothermal events at DTA curves should correspond to the end of the $M_{23}C_6$ and Cr_2N dissolution. However, the first of the above peaks appears at 890°C (888°C) and the calculated temperatures of the $M_{23}C_6$ dissolution are 934 and 960°C according to the calculations ploted in Figs. 11a and 11b, respectively. So, the diference between the experimental and calculated temperatures is 50 ÷ 70 °C. The second of the above peaks is located at 1030°C (1025°C) and the calculated temperature of the Cr_2N dissolution is 938°C for both types of calculations (the equilibrium calculation and the calculation with omitted sigma and M_6C). So, the difference between the experimental and the calculated temperatures is about

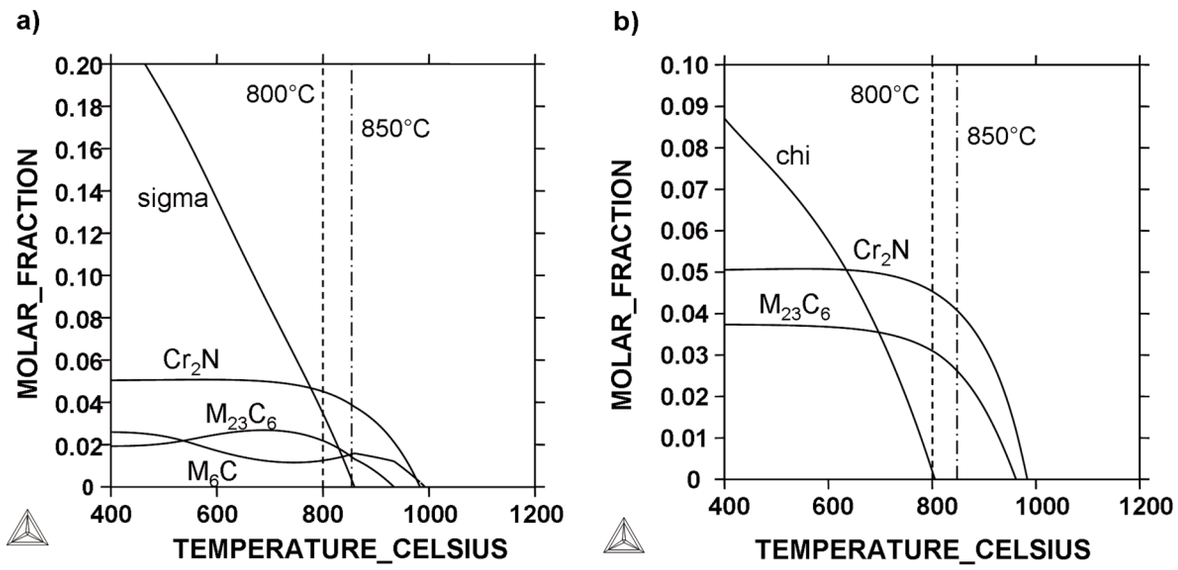

Figure 11. *Calculated molar fractions of secondary phases in dependence on temperature for the 0.17C-16Cr-11Mn-0.43N steel with equilibrium phases (a) and with sigma and M_6C phases omitted from the calculation (b). Dashed vertical lines represent positions of annealing temperatures.*

50°C in this case. It can be seen that experimental temperature of the $M_{23}C_6$ dissolution is shifted to lower temperature and the experimental temperature of the Cr_2N dissolution is shifted to higher temperature compared to the calculated values. The reason of this behaviour together with the fact that composition of chi phase was very different from the calculated value is not clear at present. Next experimental work should be focused on the chi – sigma transformation process and on modelling the phase equilibria during growth and dissolution of Cr_2N cells.

5. Conclusions

The precipitation of secondary phases was investigated in the 0.17C-16Cr-11Mn-0.43N austenitic stainless steel during annealing at 800 and 850°C for times between 5 min and 100 h. The obtained results can be summarized as follows:

1. The microstructure of the investigated high-nitrogen ASS after long-term annealing contains Cr_2N cells, $M_{23}C_6$ particles at periphery of the Cr_2N cells and at the grain boundaries. Sigma particles were found at periphery of the Cr_2N cells and the fine particles of chi phase were found inside the austenitic grains.

2. At initial stages of annealing $M_{23}C_6$, Cr_2N, and metastable chi were formed. Sigma started to precipitate after 100 h of annealing. The compositions of $M_{23}C_6$, Cr_2N and sigma during annealing were found to be close to the calculated equilibrium compositions. The composition of metastable chi differs significantly from the supposed calculated composition and this composition does not change during annealing.

3. The DTA analysis showed the initial precipitation stage followed by the dissolution of some secondary phases. In the investigated steel the computational thermodynamics could be used for qualitative interpretation of experimental results only, as the measured endothermal (dissolution) peaks are shifted about 50 ÷ 70 °C related to computed results.

Acknowledgement

The work was done in the cooperation with the Böhler Edelstahl GmbH & Co KG, Kapfenberg (Austria). The authors would like to thank for the financial support provided within the Program for Research and Development for the project Centre for Development and Application of Progressive Diagnostic Methods in the Process of Metallic and Non-metallic Material's Processing, ITMS: 26220120048, co-financed by the European Foundation for Regional Development. This study was also funded by the Grant Agency of the Ministry of Education, Science, Research, and Sport of the Slovak Republic and the Slovak Academy of Sciences (VEGA) under the contract No. 1/0339/11.

References

[1] K.H. Lo, C.H. Shek, J.K.L. Lai, Mater. Sci. Eng., R65 (2009) 39-104.

[2] R. L. Plaut, C. Herrera, D. M. Escriba, P. R. Rios, A. F. Padilha, Mater. Research, 10 (2007) 453-460.

[3] M. Milititsky, D.K. Matlock, A. Regully, N. Dewispelaere, J. Penning, H. Hanninen Mater. Sci. Eng., A496 (2008) 189-199.
[4] G. Saller, K. Spiradek-Hahn, C. Scheu, H. Clemens, Mater. Sci. Eng., A427 (2006) 246-254.
[5] T. Sourmail, Mater. Sci. Tech., 17 (2001) 1-14.
[6] J. Janovec, B. Šuštaršič, J. Medved, M. Jenko, MTAEC9, 37 (2003) 307-312.
[7] T.-H. Lee, S.-J. Kim, S. Takaki, Metall. Mater. Trans., 37A (2006) 3445-3454.
[8] T.H. Lee, C.S. Oh, C.G. Lee, S.J. Kim, S. Takaki, Scripta Mater., 50 (2004) 1325-1328.
[9] V. Gavriljuk, B.D. Shanina, H. Berns, Acta Mater., 56 (2008) 5071-5082.
[10] L. Reclaru, R. Ziegenhagen, P.-Y. Eschler, A. Blatter, J. Lemaître, Acta Biomater., 2 (2006) 433-444.
[11] K. Yang, Y. Ren, Sci. Tech. Adv. Mater., 11 (2010) 13.
[12] M. Fini, N. Nicoli Aldini, P. Torricelli, G. Giavaresi, V. Borsari, H. Lenger, J. Bernauer, R. Giardino, R. Chiesa, A. Cigada, Biomater., 24 (2003) 4929-4939.
[13] Z. Jiang, Z. Zhang, H. Li, Z. Li, Q. Ma, Mineral. Metall. Mater., 17 (2010) 729-736.
[14] M. Vach, T. Kuníková, M. Dománková, P. Ševc, Ľ. Čaplovič, P. Gogola, J. Janovec, Mater. Charac., 59 (2008) 1792–1798.
[15] M. Terada, M. Saiki, I. Costa, A.F. Padilha, Nuclear Mat., 358 (2006) 40-46
[16] D.M. Escriba, E. Materna-Morris, R.L. Plaut, A.F. Padilha, Mater. Charac., 60 (2009) 1214-1219.
[17] J. Bakajová, M. Dománková, R. Čička, S. Eglsäer, J. Janovec, Mater. Charac., 61 (2010) 969-974.
[18] C. P. O. Ossa, S. O. Rogero, A. P. Tschiptschin, Mater Sci: Mater Med., 17 (2006) 1095-1100.
[19] Yu-Xi Ma, Fan Rong, Rong Zhou, Yu-Ping Lang, Ye-Hua Jiang, Iron and Steel Res. Int., 14 (2007) 344-349.
[20] F. Vanderschaeve, R. Taillard, Mat. Sci., 30 (1995) 344-349.
[21] N.C.S. Srinivas, V.V. Kutumbarao, Scripta Mat., 51 (2004) 1105-1109.
[22] Z.Z. Yuan, Q.X. Dai, X.N. Cheng, K.M. Chen, Mater. Charac., 58 (2007) 87-91.
[23] F. Shi, Y. Qi, C. Liu, Adv. Mater. Research, 194-196 (2011) 32-37.
[24] www.thermocalc.se
[25] H.L. Lukas, S.G. Fries, B. Sundman Computational Thermodynamics. The Calphad Method. Cambridge University Press, Cambridge, 2007, p. 122-146
[26] N. Saunders, A.P. Miodownik CALPHAD. Calculation of Phase Diagrams. A Comprehensive Guide. Elsevier Science Ltd., Guildford, 1998, p. 299 - 398
[27] J. Janovec, M. Svoboda, A. Výrostková, A. Kroupa, Mater. Sci. Eng., A402 (2005) 288-293.